Quantum-classical correspondences of the Berry-Robnik parameter through bifurcations in lemon billiard systems

H. Makino,[1] T. Harayama,[2] and Y. Aizawa[1]
[1]*Department of Applied Physics, Waseda University, 3-4-1 Okubo, Shinjuku-ku, Tokyo 169-8555, Japan*
[2]*ATR Adaptive Communications Research Laboratories, 2-2 Hikaridai, Seika-cho, Soraku-gun, Kyoto 619-02, Japan*
(Received 23 October 2000; published 12 April 2001)

The quantum level statistics affected by bifurcations in classical dynamics is studied by using a one-parameter family of lemon billiard systems. The classical phase space of our system consists of regular and irregular regions. We determine an analytic solution of the phase volume for these regions as a function of the system parameter and show that the function reveals a cusp singularity at the bifurcation point. The function is compared with its quantum mechanical counterpart, the Berry-Robnik parameter. By estimating the semiclassical regime from the effective Planck constant that validates the quantum-classical correspondence of the Berry-Robnik parameter, we determine a region of the system parameter where the cusp can be reproduced by the statistical properties of the eigenenergy levels.

DOI: 10.1103/PhysRevE.63.056203 PACS number(s): 05.45.Mt, 03.65.Sq

I. INTRODUCTION

An important correspondence between classical and quantum mechanics is observed in the statistical properties of energy levels. As is well known, universal classes appear in spectral fluctuations that are characterized by a level spacing distribution; the level spacing distribution of an integrable case is characterized by the Poisson distribution [1,2], and that of a strongly chaotic system is characterized by the Wigner distribution [3,4]. Furthermore, the transition from the Poisson distribution to the Wigner distribution is observed in mixed systems where classical phase space consists of regular (quasiperiodic) and irregular (chaotic) regions [5–9]. Berry and Robnik surmised that the energy levels of mixed systems consist of two separate sequences, the Poisson distributed sequence and the Wigner distributed sequence [10]. The relative weights of these two sequences, ρ_1 and ρ_2 $(\rho_1+\rho_2=1)$, are assumed to be the relative Liouville measures of the regular and irregular regions on in the energy surface. The simple superposition of the two level sequences, neglecting interactions between them, yields the Berry-Robnik formula,

$$P^{\mathrm{BR}}(\rho_1,\rho_2;S)=C\frac{d^2}{dS^2}\left[\exp(-\rho_1 S)\,\mathrm{erfc}\left(\frac{\sqrt{\pi}}{2}\rho_2 S\right)\right], \tag{1.1}$$

where S is the level spacing, C is a constant value that is determined by the normalization condition, $\int_0^\infty P_K^{\mathrm{BR}}(S)=1$, and $\mathrm{erfc}(x)$ is the error function,

$$\mathrm{erfc}(x)=\frac{2}{\sqrt{\pi}}\int_x^\infty \exp(-t^2)\,dt. \tag{1.2}$$

This formula can bridge the gap between the Poisson distribution $(\rho_1=0,\rho_2=1)$,

$$P^{\mathrm{BR}}(1,0;S)=e^{-S} \tag{1.3}$$

and the Wigner distribution $(\rho_1=1,\rho_2=0)$,

$$P^{\mathrm{BR}}(0,1;S)=\tfrac{1}{2}\pi S e^{-(\pi/4)S^2}. \tag{1.4}$$

It was verified that the formula (1.1) can, with great accuracy, reproduce the numerical data for the level spacing distribution in the very high energy region, i.e., the semiclassical energy region, where the effective Planck constant is negligible in comparison with the volume ratio of structures in the classical phase space [11–18]. This formula associates the level spacing distribution of the quantum system with the geometry of the classical phase space that is affected by the bifurcation. This means that the bifurcation of the classical dynamical system can be detected by quantum level statistics. However, only a few attempts have been made thus far to study the interrelation between the bifurcation and the energy level statistics.

In a previous paper dealing with oval billiard systems [19], we demonstrated that the effect of bifurcations in classical Hamiltonian dynamics appears clearly in the energy level statistics of the corresponding quantum system. That is, the quantum mechanical value of the Berry-Robnik parameter obtained by fitting the level spacing distribution to the Berry-Robnik formula had a significant dependence on a system parameter due to bifurcation. Figure 1 shows the Berry-Robnik parameter $\rho_2^q(\delta)$ where the horizontal δ axis represents the system parameter and δ_c is the point of the bifurcation. The Berry-Robnik parameter drops suddenly at the bifurcation point and has a dip at δ_c. The purpose of this paper is to analyze this singularity of the Berry-Robnik parameter at the bifurcation point $\delta=\delta_c$.

In the oval billiard, the classical phase space is too complicated to deal with at the bifurcation point precisely because a second chaotic region appears [19]. For this reason, in this paper we deal with a simplified model called the lemon billiard. The wall of this system has partially the same boundary geometry as that of the oval billiard, so that there appears the identical bifurcation at δ_c.

The lemon billiard was first introduced by Heller and Tomsovic [20] and studied by Ree and Reichl [21]. The shape of the billiard depends on the value of one parameter.

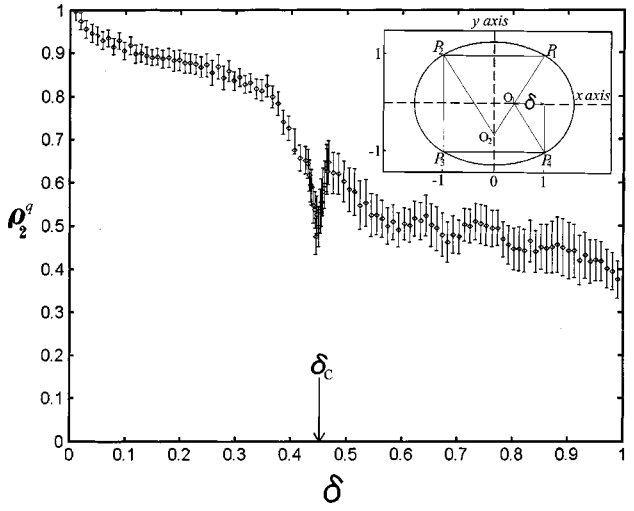

FIG. 1. The Berry-Robnik parameter $\rho_2^q(\delta)$ versus the system parameter δ for quantum oval billiards [19]. δ_c on the horizontal axis is the bifurcation parameter point.

As the parameter is varied, the system changes continuously from integrable to nonintegrable. The transition is accompanied by successive bifurcations, i.e., the creation and disappearance of a periodic orbit which has a great impact on the phase space structures.

The present paper is organized as follows. The lemon billiard is introduced in Sec. II, and Sec. III involves an analysis of the Poincaré surface of section where the bifurcation parameter is determined. In Sec. IV, the stability of the linearized Poincaré mapping is analyzed for the bifurcating orbit. In Sec. V, volume ratios (relative measures of the phase space components on the Poincaré surface of section) are determined analytically and characteristic structures induced by the bifurcation are also analyzed. In Sec. VI, the volume ratios are compared with the quantum mechanical data for the Berry-Robnik parameter, and the Berry-Robnik parameter in the vicinity of the bifurcation point is precisely analyzed in Sec. VII.

II. LEMON BILLIARDS

Figure 2 shows the schematic definition of the lemon billiard. The wall ∂D for the billiard is constructed as follows. In a rectangular system of coordinates (x,y), we consider four points P_1,P_2,P_3, and P_4 with coordinates (1,1), $(-1,1)$, $(-1,-1)$, and $(1,-1)$, respectively, forming a square with side length 2. Let the point with coordinate $(1-\delta, 0)$ be denoted P_0, where δ is defined in the interval $0<\delta\leqslant 1$. O_1 is the intersection of the extension of P_1P_0 and the y axis, and it is the center of an arc $\widehat{P_1P_2}$. The wall ∂D of the billiard consists of the above arc and another arc, $\widehat{P_3P_4}$, constructed similarly. The initial condition of the motion of a particle is determined by its position and direction.

The shape of the billiard wall depends on the value of δ. In the case $\delta=1$, the shape of the billiard wall is circular, and the billiard system is completely integrable. The motion of the particle is regular for any choice of the initial condition. In the parameter region $0<\delta<1$, the billiard system is nonintegrable and softly chaotic, where the motion of the particle can be regular or irregular depending on the initial condition. As the parameter is varied, the system makes a transition from integrable to nonintegrable with successive bifurcations.

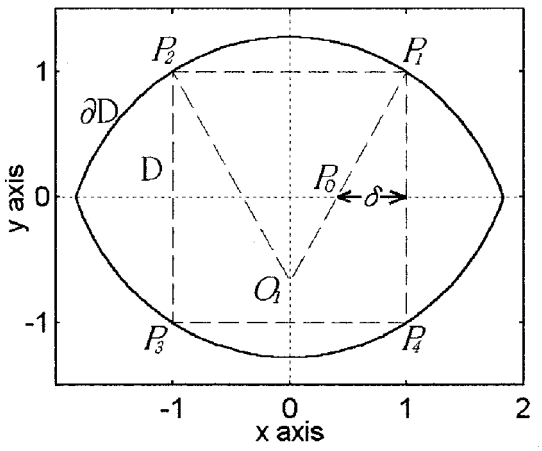

FIG. 2. Schematic picture of the lemon billiard whose boundary wall ∂D consists of two circular arcs. The parameter δ is defined in the interval $0<\delta\leqslant 1$.

Since the lemon billiard is a simplified model of the oval billiard, the geometry of its boundary wall is partially identical to that of the oval billiard, so that the same bifurcation of the periodic orbit bouncing between the regions $\widehat{P_1P_2}$ and $\widehat{P_1P_2}$ can be actualized in the lemon billiard as well.

III. BIFURCATION

We consider the successive collisions of a particle with the wall ∂D and define the Birkhoff coordinates $(\phi,\sin\alpha)$ as shown in Fig. 3, where ϕ is the normalized curvilinear distance measured along the wall from the origin A to the collisional point B, and α is the angle between the inner normal and the orbit reflected from the wall ∂D. The Birkhoff coordinates are the most natural representation of Poincaré surface of a section for billiard systems and describe the global behavior of the motions [22].

Figure 4 shows the trajectories in Birkhoff coordinates for various values of δ. In the cases of $\delta=1$ (circle) and $\delta=\delta_c=(4-\sqrt{7})/3$, the whole surface of section is completely filled with regular and irregular orbits, respectively. In all cases of $0<\delta<\delta_c$ and $\delta_c<\delta<1$, regular and irregular re-

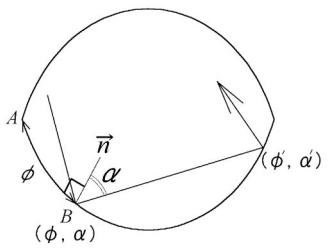

FIG. 3. Definition of the Birkhoff coordinates $(\phi, \sin\alpha)$.

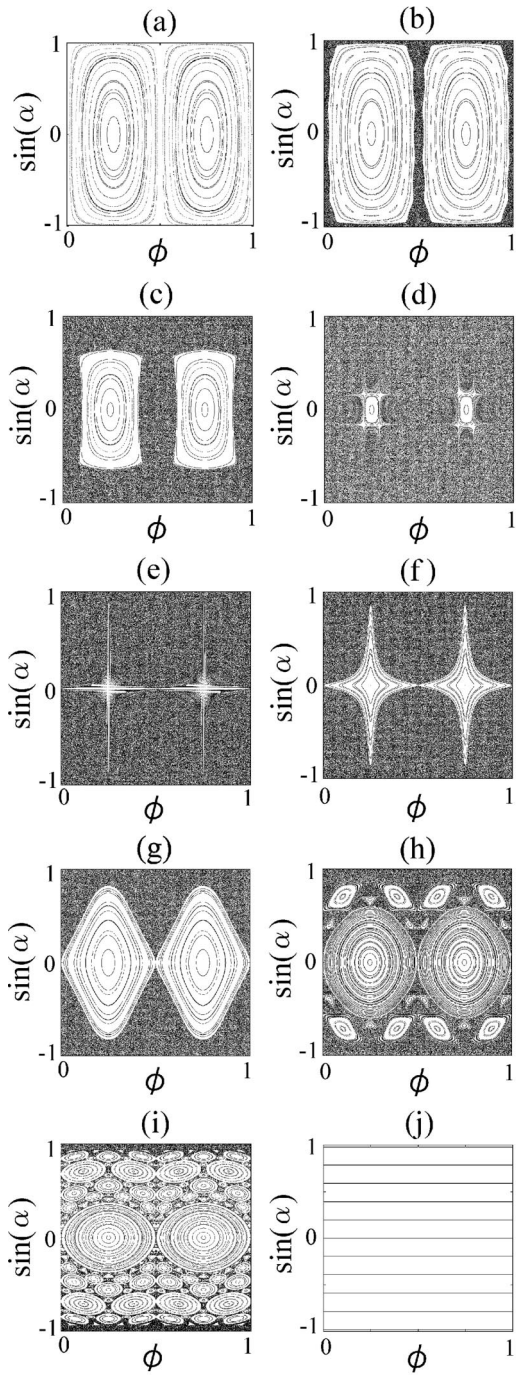

FIG. 4. Poincaré surfaces of section for $\delta=$ (a) 0.00001, (b) 0.04, (c) 0.35, (d) 0.445, (e) 0.451 416 229 (δ_c), (f) 0.452, (g) 0.5, (h) 0.75, (i) 0.9, and (j) 1.

gions coexist in the Poincaré surface of section.

As δ increases from 0, one can observe the gradual enhancement of an irregular region around two island tori centered at elliptic fixed points ($\phi=0.5\pm0.25,\sin\alpha=0$), as shown in Figs. 4(a)–4(c). But the sizes of these island tori suddenly change in the parameter region above the critical point δ_1,

$$\delta_1=2-\sqrt{3}, \tag{3.1}$$

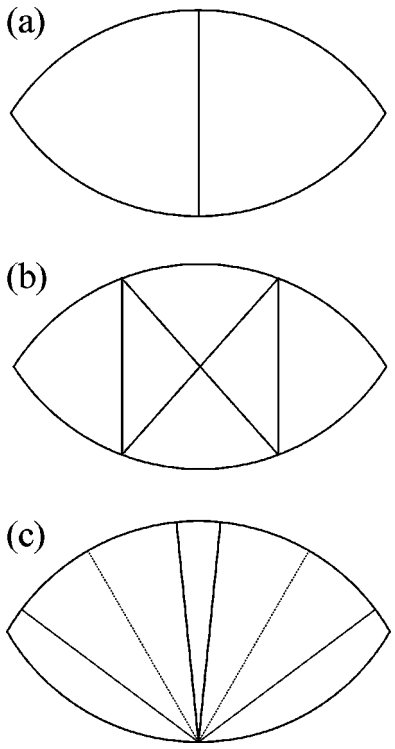

FIG. 5. (a) An elliptic periodic orbit with a period of 2 at $\delta=0.4$. (b) A hyperbolic periodic orbit with a period of 4 at $\delta=0.4$. (c) Neutral periodic orbits with period 4 at $\delta=\delta_c$.

where a hyperbolic periodic orbit, as shown in Fig. 5(b), appears suddenly at $\phi=0$ and 0.5. In the parameter region $\delta>\delta_1$, the corresponding hyperbolic fixed points with a period of 4 compose a Poincaré Birkhoff chain with the elliptic fixed points with a period of 2 that are mentioned above.

As δ increases further, these hyperbolic periodic points at ($\phi\equiv\phi_{\bowtie}^{\pm}$, $\sin\alpha\equiv\sin\alpha_{\bowtie}^{\pm}$),

$$\phi_{\bowtie}^{\pm\pm}(\delta)=\frac{1}{2}\pm\frac{1}{4}+\frac{\alpha_{\bowtie}^{\pm}}{4\arctan[\sqrt{2\delta}/(1-\delta)]},$$
$$\sin\alpha_{\bowtie}^{\pm}=\pm\frac{\sqrt{3\delta^2-8\delta+3}}{2(1-\delta)}, \tag{3.2}$$

push the island tori toward the elliptic fixed points at ($\phi=0.5\pm0.25,\sin\alpha=0$), as shown in Figs. 4(c)–4(e).

When δ is equal to another critical point δ_c,

$$\delta_c=\frac{4-\sqrt{7}}{3}. \tag{3.3}$$

Here one can see a bifurcation where the hyperbolic fixed points mentioned above collide with the elliptic points at ($\phi=0.5\pm0.25,\sin\alpha=0$) as shown in Figs. 4(e), and simultaneously these fixed points disappear through the bifurcation process. As a consequence, the whole surface of section is filled with a chaotic orbit at $\delta=\delta_c$. Thus one can observe a sudden decrease in the size of the island tori between δ_1 and δ_c, as shown in Figs. 4(c)–4(e). We have summarized

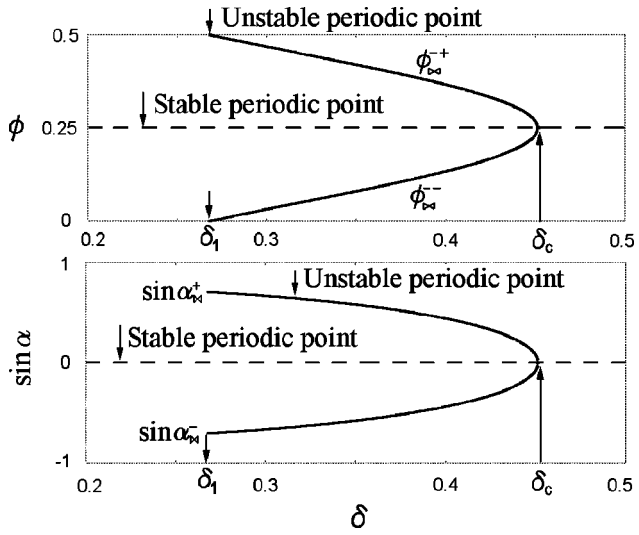

FIG. 6. Bifurcation diagram in which the solid curve represents unstable periodic points and the dashed line represents a stable periodic point.

the above bifurcation process in diagrams, as shown in Fig. 6. $\delta=\delta_c$ is the special critical point where the center O_1 of the arc $\widehat{P_1P_2}$ is just at $\phi=0.25$ on the opposite arc $\widehat{P_3P_4}$, so that a family of periodic orbits with a period of 4 appears, as shown in Fig. 5(c), all along the lines $\phi=0.25$ and $\phi=0.75$ on the Poincaré surface of section.

In the parameter region $\delta>\delta_c$, elliptic fixed points with a period of 2 are created again at $(\phi=0.5\pm0.25,\sin\alpha=0)$ as shown in Fig. 4(f), and as a result the phase volume of the regular region increases again.

Furthermore, numerous bifurcations appear in addition to the one mentioned above that correlate with the creation and disappearance of various periodic orbits. We summarize the parameter values for some typical bifurcations in Appendixes A and B. The bifurcation at $\delta=\delta_c$ has the strongest impact on the phase space structures among these bifurcations since this bifurcation induces the creation and disappearance of the periodic orbit with a period of 2 that is closely associated with the largest island tori in the phase space. In this paper, we focus our attention on this bifurcation in the following sections.

IV. STABILITY ANALYSIS OF BIFURCATING PERIODIC ORBIT

Here we linearize the Poincaré mapping and analyze the stability of the periodic points with a period of 2 at $(\phi=0.5\pm0.25,\sin\alpha=0)$.

The $(n+1)$th iterated point on the Poincaré surface of section is obtained from the previous nth point as $\phi_{n+1}=\phi_{n+1}(\phi_n,\sin\alpha_n)$ and $\sin\alpha_{n+1}=\sin\alpha_{n+1}(\phi_n,\sin\alpha_n)$. Therefore, the Poincaré mapping is linearized in the vicinity of the point $(\phi_0,\sin\alpha_0)$ as follows:

$$\Delta\phi_{n+1}=\left.\frac{\partial\phi_{n+1}}{\partial\phi_n}\right|_{(\phi_0,\sin\alpha_0)}\Delta\phi_n+\left.\frac{\partial\phi_{n+1}}{\partial\sin\alpha_n}\right|_{(\phi_0,\sin\alpha_0)}\Delta\sin\alpha_n, \tag{4.1}$$

$$\Delta\sin\alpha_{n+1}=\left.\frac{\partial\sin\alpha_{n+1}}{\partial\phi_n}\right|_{(\phi_0,\sin\alpha_0)}\Delta\phi_n+\left.\frac{\partial\sin\alpha_{n+1}}{\partial\sin\alpha_n}\right|_{(\phi_0,\sin\alpha_0)}\Delta\sin\alpha_n. \tag{4.2}$$

In the lemon billiard system, the linearized Poincaré mapping in the vicinity of the fixed point at $(\phi=0.5\pm0.25,\sin\alpha=0)$ is described by using the 2×2 monodromy matrix as

$$\begin{pmatrix}\Delta\phi_{n+2}\\ \Delta\sin\alpha_{n+2}\end{pmatrix}=M(\delta)\begin{pmatrix}\Delta\phi_n\\ \Delta\sin\alpha_n\end{pmatrix} \tag{4.3}$$

where

$$M(\delta)=\begin{pmatrix}\left.\frac{\partial\phi_{n+2}}{\partial\phi_{n+1}}\right|_{(0.75,0)} & \left.\frac{\partial\phi_{n+2}}{\partial\sin\alpha_{n+1}}\right|_{(0.75,0)}\\ \left.\frac{\partial\sin\alpha_{n+2}}{\partial\phi_{n+1}}\right|_{(0.75,0)} & \left.\frac{\partial\sin\alpha_{n+2}}{\partial\sin\alpha_{n+1}}\right|_{(0.75,0)}\end{pmatrix}\begin{pmatrix}\left.\frac{\partial\phi_{n+1}}{\partial\phi_n}\right|_{(0.25,0)} & \left.\frac{\partial\phi_{n+1}}{\partial\sin\alpha_n}\right|_{(0.25,0)}\\ \left.\frac{\partial\sin\alpha_{n+1}}{\partial\phi_n}\right|_{(0.25,0)} & \left.\frac{\partial\sin\alpha_{n+1}}{\partial\sin\alpha_n}\right|_{(0.25,0)}\end{pmatrix} \tag{4.4}$$

$$=\begin{pmatrix}2[2w(\delta)-1]^2-1 & 4w(\delta)[1-2w(\delta)]R(\delta)\\ 4[(2w(\delta)-1)(1-w(\delta)]/R(\delta) & 2[2w(\delta)-1]^2-1\end{pmatrix}, \tag{4.5}$$

with

$$w(\delta)=1-\frac{1-\delta}{\sqrt{1+\delta^2}},\quad R(\delta)=\frac{\sqrt{1+\delta^2}}{\delta}. \tag{4.6}$$

The stability of the periodic points at $(\phi=0.5\pm0.25,\sin\alpha=0)$ can be estimated from eigenvalues of the monodromy matrix $M(\delta)$ [23,24], $\lambda_\pm$, which are given in terms of the trace of $M(\delta)$ as follows:

$$\lambda_\pm(\delta)=\frac{1}{2}(\mathrm{Tr}\,M(\delta)\pm\{[\mathrm{Tr}\,M(\delta)]^2-4\}^{1/2}). \tag{4.7}$$

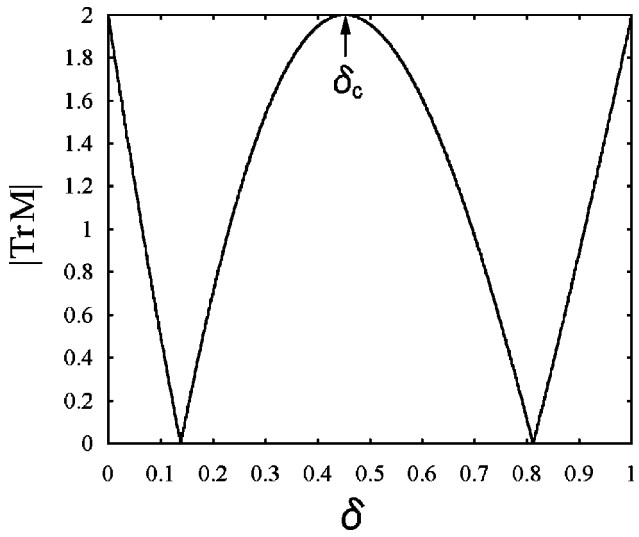

FIG. 7. The trace of the monodromy matrix $|\mathrm{Tr}\, M(\delta)|$.

The orbit is stable, unstable, and neutral when $|\mathrm{Tr}\, M|<2$, $|\mathrm{Tr}\, M|>2$, and $|\mathrm{Tr}M|=2$, respectively. Thus, as shown in Fig. 7, the periodic points under consideration are stable when $0<\delta<\delta_c$, $\delta_c<\delta<1$ and neutral when $\delta=0$, δ_c, and 1. Note that the periodic points are neutral just at the bifurcation point $\delta=\delta_c$, and that periodic orbits with a period of 4, as shown in Fig. 5(c), appear only at the bifurcation point for various reflection angles α at $\phi=0.25$ and 0.75. These neutral periodic points compose a family of bouncing periodic orbits as shown in Fig. 8.

V. ANALYSIS OF CUSP AT THE BIFURCATION POINT

In this section, we analyze the volume ratio of the regular and chaotic regions on the Poincaré surface of section.

Figure 9 shows numerical plots of the volume ratio of the irregular region. The ratio $\rho_2(\delta)$ is obtained by using a numerical method introduced in Ref. [19]. The ratio $\rho_2(\delta)$ shows sudden increases at various parameter points. These points of increase correspond to bifurcation parameters; we give some of these parameter values in Appendixes A and B. The ratio $\rho_2(\delta)$ at the parameter point $\delta=\delta_c$ shows a significant structure due to the bifurcation. Here let us analyze the precise structure of this function at $\delta=\delta_c$.

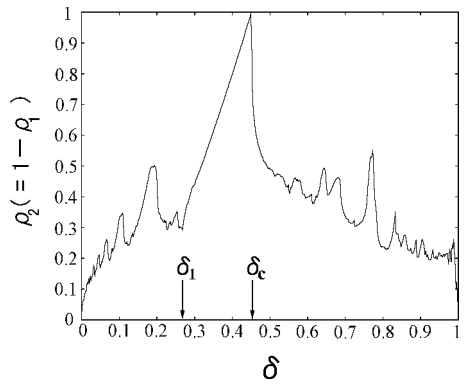

FIG. 9. Numerical plots of $\rho_2(\delta)$.

The phase space in the region $\delta_1<\delta<\delta_c$ consists of island tori centered at $(\phi=0.5\pm0.25,\sin\alpha=0)$ and a single chaotic sea, as shown in Fig. 4(e), so that the total volume ratio of the regular region $\rho_1(=1-\rho_2)$ is calculated effectively only from the contributions of the island tori. These island tori are encircled by the unstable periodic points at $(\phi_{\bowtie}^{\pm\pm},\sin\alpha_{\bowtie}^{\pm})$. In the parameter region $\delta_1\leqslant\delta\leqslant\delta_c$ the outer bound surface of the island torus is approximated successfully by a rectangle. The two sides of this rectangle are denoted by *A* and *B*, and the lengths of these sides are given by the distances between the unstable periodic points as follows:

$$A(\delta)=\phi_{\bowtie}^{-+}-\phi_{\bowtie}^{--}=\phi_{\bowtie}^{++}-\phi_{\bowtie}^{+-}=\frac{\arcsin\, B(\delta/2)}{2\arctan[\sqrt{2\delta}/(1-\delta)]}, \tag{5.1}$$

$$B(\delta)=\sin\alpha_{\bowtie}^{+}-\sin\alpha_{\bowtie}^{-}=\frac{\sqrt{3\delta^2-8\delta+3}}{1-\delta}. \tag{5.2}$$

Therefore the ratios ρ_1 and ρ_2 can be determined approximately as functions of δ as follows:

$$\rho_1(\delta)\simeq A(\delta)\times B(\delta),\quad \delta_1\leqslant\delta\leqslant\delta_c, \tag{5.3}$$

$$\rho_2(\delta)=1-\rho_1(\delta). \tag{5.4}$$

Note that $\rho_1(\delta)$ decreases toward 0 as $\delta\to\delta_c$.

Here let us focus our attention on the parameter dependence of $\rho_1(\delta)$ and $\rho_2(\delta)$ in the neighborhood of the bifurcation point $\delta=\delta_c$. Equations (5.1) and (5.2) can be expanded by describing $\delta\equiv\delta_c-\epsilon$ for small ϵ $(\ll\delta_c)$ as

$$A=\frac{\sqrt{8-6\delta_c}}{4(1-\delta_c)\arctan[\sqrt{2\delta_c}/(1-\delta_c)]}\epsilon^{1/2}+O(\epsilon^{3/2}), \tag{5.5}$$

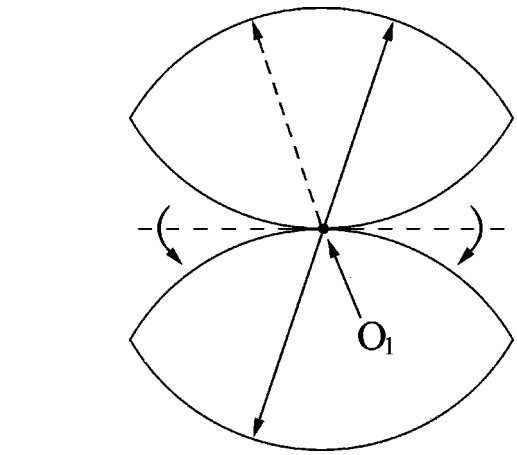

FIG. 8. Schematic picture of a periodic orbit that appears only at the bifurcation point $\delta=\delta_c$. The periodic orbits, which pass through the point O_1 on the symmetry line, compose a family of bouncing ball orbits.

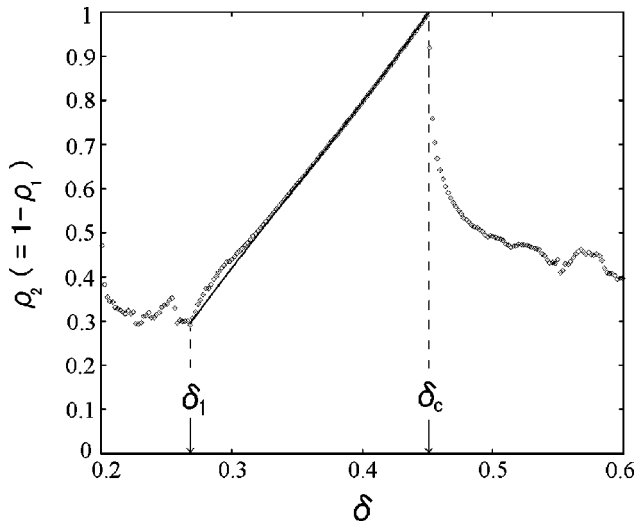

FIG. 10. Comparison of $\rho_2(\delta)$ between an analytic curve and numerical plots in the vicinity of the bifurcation point at $\delta=\delta_c$. We have not yet succeeded in determining an analytic solution for $\rho_2(\delta)$ in the parameter region $\delta \geqslant \delta_c$.

$$B=\frac{\sqrt{8-6\delta_c}}{2(1-\delta_c)}\epsilon^{1/2}+O(\epsilon^{3/2}), \tag{5.6}$$

and hence Eqs. (5.3) and (5.4) can be rewritten as

$$\rho_1(\epsilon)=c(\delta_c)\epsilon+O(\epsilon^2), \tag{5.7}$$

$$\rho_2(\epsilon)=1-\rho_1(\epsilon), \tag{5.8}$$

where

$$c(\delta_c)=\frac{4-3\delta_c}{2(1-\delta_c)^2\arctan[\sqrt{2\delta_c}/(1-\delta_c)]}. \tag{5.9}$$

It should be noted that $\rho_1(\delta)$ at the bifurcation point is a cusp since the constant term does not appear in the above expansion (5.7), while the expansion coefficient of the first order term does not vanish, and hence $\rho_1(\epsilon)$ at the bifurcation point is a linear curve.

The above analytic solution (5.3), depending on the approximation by the rectangle, is validated numerically. Figure 10 shows schematic comparisons of $\rho_2(\delta)$ between an analytic curve of Eq. (5.4) and numerical plots in the interval $\delta_1 \leqslant \delta \leqslant \delta_c$. The numerical plots are obtained by using the method introduced in Ref [19]. One can see that the numerical data fit the analytic curve well in the parameter region between δ_1 and δ_c and reproduce the linearity of Eq. (5.7) with a high degree of accuracy. Thus we see that the approximation of Eq. (5.3) is validated numerically and that the analytic curves $\rho_1(\delta)$ and $\rho_2(\delta)$ almost completely reproduce, respectively, the regular and chaotic regions in the phase space between δ_1 and δ_c.

VI. THE BERRY-ROBNIK PARAMETER AT THE BIFURCATION POINT

Here we compare the volume ratio ρ_i of the phase space component with the quantum mechanical data for the Berry-Robnik parameter ρ_i^q.[1] Figures 11(a)–11(c) show schematic comparisons between $\rho_2(\delta)$ and $\rho_2^q(\delta)$ for various energy ranges where n is the level number of a desymmetrized eigenstate with odd-odd parity. The Berry-Robnik parameter is obtained by fitting the level spacing distributions $P(S)$ of the quantum lemon billiard to the Berry-Robnik formula (1.1), where the fitting parameter ρ_i^q is determined by the least squares method for the cumulative level spacing distribution $W(S)=\int_0^S P(S')dS'$. One can see that the quantum mechanical value $\rho_2^q(\delta)$ clearly reproduces the global enhancement of $\rho_2(\delta)$ in the neighborhood of the bifurcation point. However, a large deviation exists between $\rho_2^q(\delta)$ and $\rho_2(\delta)$ in the low energy ranges, as shown in Figs. 11(a) and 11(b). This is because the Berry-Robnik formula is applicable only in the so-called semiclassical regime in the high energy region where the effective Planck constant $h_{\rm eff}(n)$,

[1]The relationship between the relative measure ρ_2 on the Poincaré surface of section and the relative Liouville measure on the energy surface is explained in Sec. VIII.

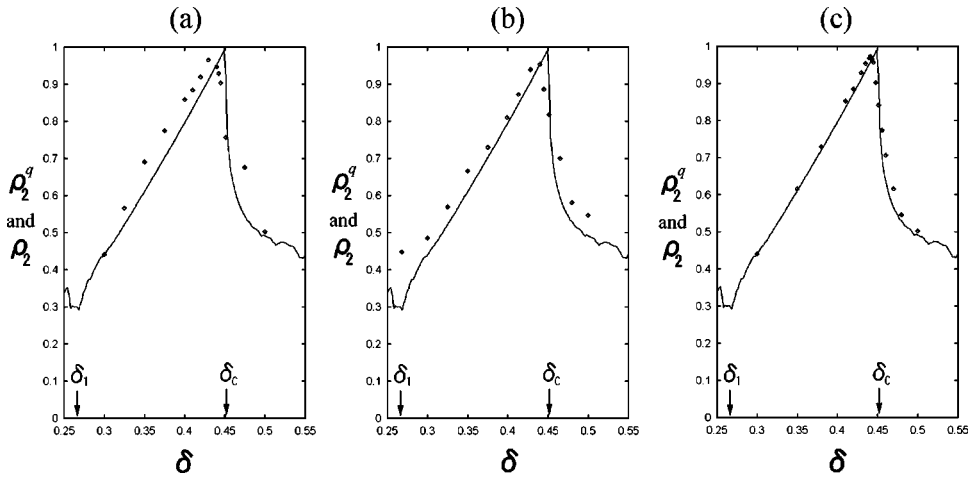

FIG. 11. Schematic comparison between the Berry-Robnik parameter $\rho_2^q(\delta)$ ($\diamond$) and the volume ratio of the chaotic region $\rho_2(\delta)$ (solid curve) for various energy ranges. In each case, we used 2000 eigenenergy levels E_n with (a) $n \in [2001,4000]$, (b) $n \in [8001,10\,000]$, and (c) $n \in [17\,001,19\,000]$ which have odd-odd parity. The quantum mechanical value $\rho_2^q(\delta)$ is calculated effectively by the boundary element method [26].

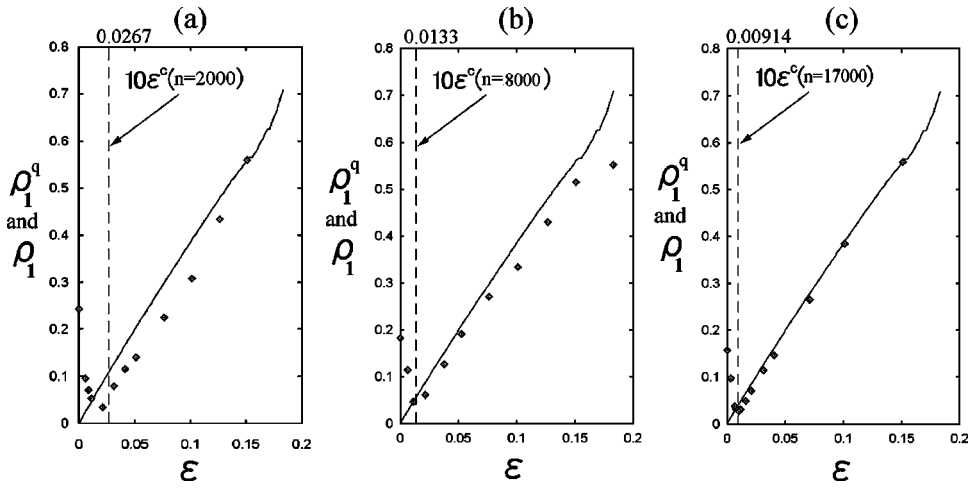

FIG. 12. Schematic comparison between the Berry-Robnik parameter $\rho_1^q(\epsilon)$ ($\diamond$) and the analytic curve of the volume ratio $\rho_1(\epsilon)$ near the bifurcation point $\epsilon=0$. In each case, 2000 eigenenergy levels E_n are used with (a) $n\in[2001,4000]$, (b) $n\in[8001,10000]$, and (c) $n\in[17\,001,19\,000]$ with odd-odd parity.

$$h_{\rm eff}(n)\simeq\frac{1}{\sqrt{4n}}, \tag{6.1}$$

is sufficiently smaller than the volume ratio of the island tori [16],

$$(n,\delta)\in\{h_{\rm eff}(n)\ll\rho_1(\delta)\}, \tag{6.2}$$

the Berry-Robnik parameter in the low energy range does not agree with the counterpart in the classical dynamical system. Accordingly, the deviation between $\rho_2^q(\delta)$ and $\rho_2(\delta)$ becomes smaller as the energy range of the quantum system becomes much higher, as shown in Figs. 11(b) and 11(c).

It is noteworthy that there is still a large deviation between $\rho_2^q(\delta)$ and $\rho_2(\delta)$ in the neighborhood of the bifurcation point, i.e., the Berry-Robnik parameter at the bifurcation point is blunt while the volume ratio of the chaotic region in the classical dynamical system is cuspidal.

Figures 12(a)–12(c) compare the volume ratio of the regular region $\rho_1(\epsilon)$ and the Berry-Robnik parameter $\rho_1^q(\epsilon)$ in the neighborhood of the bifurcation point at $\epsilon=0$. Here we have to remember that the ratio $\rho_1(\epsilon)$ has a linear dependence on the system parameter ϵ as shown in Eq. (5.7). One can see that there is a large deviation between $\rho_1(\epsilon)$ and $\rho_1^q(\epsilon)$ in the neighborhood of the bifurcation point and that the linear dependence on the system parameter is not reproduced by the quantum mechanical value of the Berry-Robnik parameter. This means that the Berry-Robnik formula does not work at all in the vicinity of the bifurcation point. The above disagreement is analyzed in the next section.

VII. QUANTUM MECHANICAL LIMITS IN RESOLUTION OF THE BERRY-ROBNIK PARAMETER

In the last section, we showed numerically that the Berry-Robnik parameter does not agree with the volume ratio of the classical phase space in the neighborhood of the bifurcation point. Although the volume ratio of the classical dynamical system, $\rho_i, i=1,2$, at the bifurcation point showed a cuspidal structure and a linear dependence on the system parameter, the quantum mechanical counterparts, the Berry-Robnik parameter $\rho_i^q, i=1,2$, could not reproduce these characteristic structures at the bifurcation point $\epsilon=0$ or $\delta=\delta_c$. This is because the size of the island region decreases toward 0 as $\epsilon\to0$, and the quantum system at the bifurcation point cannot satisfy the condition of Eq. (6.2) while in the finite energy range, $n\ll\infty$,

$$\lim_{\epsilon\to0}\rho_1(\epsilon)\simeq\lim_{\epsilon\to0}c(\delta_c)\epsilon=0. \tag{7.1}$$

Therefore, the Berry-Robnik formula in the finite energy range does not work effectively in the neighborhood of the bifurcation point. The condition $\rho_1(\epsilon)=h_{\rm eff}(n)$ for a given energy level n gives a critical value of the system parameter ϵ which is calculated from Eq. (5.3), Eq. (6.1), and $\epsilon=\delta_c-\delta$ as follows:

$$\epsilon^c(n)=\delta_c-\rho_1^{-1}(h_{\rm eff}(n)). \tag{7.2}$$

In the region near the bifurcation point, $0<\epsilon<\epsilon^c(n)$ [or $\delta_c-\epsilon^c(n)<\delta<\delta_c$], quantum systems cannot resolve the island regions since $h_{\rm eff}(n)>\rho_1$. The sizes of island regions are beyond the maximum ability of the resolution by the quantum eigenstate, so that the Berry-Robnik formula is not applicable to the quantum system. This means that the Berry-Robnik parameter ρ_1^q is not guaranteed to reproduce ρ_1. On the other hand, in the parameter region $\epsilon>\epsilon^c(n)$ [or $\delta<\delta_c-\epsilon^c(n)$], the quantum system can resolve the island region since the effective Planck constant is smaller than the size of the island region, $h_{\rm eff}(n)<\rho_1(\epsilon)$. In the parameter region $\epsilon\gg\epsilon^c(n)$ the Berry-Robnik formula works well since the effective Planck constant is sufficiently smaller than the size of the island region, $h_{\rm eff}(n)\ll\rho_1$. Therefore, one can observe in the parameter region near the bifurcation point $\epsilon=0$ that the quantum mechanical value $\rho_i^q(\epsilon)$ cannot reproduce its counterpart in the classical dynamical system, $\rho_i(\epsilon)$.

Figures 12(a)–12(c) show schematic comparisons between the Berry-Robnik parameter for various energy regions $\rho_1^q(\epsilon)$ and the analytic curve of the ratio $\rho_1(\epsilon)$ given by Eq. (5.3). In each figure, the vertical dotted line represents $10\epsilon^c(n)$. One can see that $\rho_1^q(\epsilon)$ agrees with $\rho_1(\epsilon)$ in the region $\epsilon\gg\epsilon^c(n)$. On the other hand, a large deviation appears between them near the origin $\epsilon=0$. Note that the cus-

TABLE I. The Berry-Robnik parameter at the bifurcation point, $\rho_1^q(\delta_c)$, for various ranges of energy levels.

n	$\rho_1^q(\delta_c)=1-\rho_2^q$
2001–4000	0.243
8001–10000	0.182
17001–19000	0.157
33001–35000	0.093
52001–54000	0.072

pidal structure in the vicinity of the bifurcation point cannot be reproduced by the quantum mechanical Berry-Robnik parameter at all. One can see that the blunt region near the origin, $0 \leqslant \epsilon \leqslant 10\epsilon^c(n)$, gets smaller as the energy of the system gets higher. This is because $\epsilon^c(n)$ decreases to 0 as $n \to \infty$,

$$\lim_{n\to\infty} \epsilon^c(n) \approx \lim_{n\to\infty} \frac{1}{c(\delta_c)} \frac{1}{\sqrt{4n}} = 0, \tag{7.3}$$

so that the blunt region diminishes in width in the semiclassical limit. Table I shows the Berry-Robnik parameter at the bifurcation point for various energy ranges. The Berry-Robnik parameter $\rho_1^q(\delta_c)$ does not agree with the volume ratio $\rho_1(\delta_c)(=0)$ in any energy range, and the deviation from this ratio is very large in the low energy range. However, the deviation at the origin becomes smaller as the energy of the quantum system gets higher, and the Berry-Robnik parameter agrees with the volume ratio better in the high energy ranges than in the low energy ranges. Therefore, one can see that the Berry-Robnik parameter can reproduce the cuspidal structure of the function $\rho_i(\delta)$ at $\delta=\delta_c$ more precisely in the higher energy region and that the quantum mechanical Berry-Robnik parameter $\rho_1^q(\epsilon)$ reproduces the linear dependence of $\rho_1(\epsilon)$ on ϵ very well in the semiclassical regime, as shown in Eq. (6.2). This result means that the statistical properties of energy levels in the high energy range can be reflected sensitively by the local enhancement of island tori in the classical phase space whose volume ratios are controlled by the periodic orbit at $(\phi_{\bowtie}^{\pm\pm}, \sin\alpha_{\bowtie}^{\pm})$.

VIII. SUMMARY AND DISCUSSION

In this paper, we analyzed the quantum mechanical Berry-Robnik parameter, which is affected by a bifurcation of the classical dynamical system. We revealed the detailed structure of the Berry-Robnik parameter at the bifurcation point, i.e., the Berry-Robnik parameter in the semiclassical energy region was shown to have a linear dependence on the system parameter in the vicinity of the bifurcation point and to be cuspidal just at the bifurcation point.

The quantum Berry-Robnik parameter, which was obtained by applying the Berry-Robnik formula to the level spacing distribution, agreed well with the classical volume ratio (the relative measure of the phase space components on the Poincaré surface of section) in the high energy range and was greatly affected by the bifurcation. Thus we were able to analyze the Berry-Robnik parameter in terms of the classical volume ratio.

First, the phase volume of the regular and chaotic regions in the classical phase space was determined analytically as a function of the system parameter. Using the unstable periodic orbit, the total phase volume of the island tori could be approximated successfully with rectangles, and could be characterized as a function of the system parameter. The volume function was expanded by a small parameter in the vicinity of the bifurcation point. We were able to show that the volume function was cuspidal just at the point of the bifurcation since the constant term in the expansion series vanished, and that the volume function had a linear dependence on the system parameter near the bifurcation point since the expansion coefficient of the first order term did not vanish. Therefore, we were able to determine the structure of the volume ratio at the bifurcation point.

Secondly, we numerically checked the above analytic results for the volume ratio of the classical phase space. The volume ratios of the regular and chaotic regions agreed well with the numerical results of these regions. Thus, the approximation part of the analytic derivation was numerically validated.

Thirdly, the quantum mechanical data Berry-Robnik parameter was compared with the volume ratio of the classical phase space in the vicinity of the bifurcation point. However, a large deviation appeared between them; the Berry-Robnik parameter at the bifurcation point was blunt and could not precisely reproduce the cuspidal structure of the volume ratio and linearity. This is because the Berry-Robnik formula truly describes the quantum level statistics only in the extra deep semiclassical regime (or high energy region), while in the low energy range it does not work well since the quantum eigenstate cannot resolve the detailed structure in the phase space. We compared the effective Planck constant with the phase volume of the island tori that we determined analytically, and derived as a function of the level number n the characteristic threshold of the system parameter $\epsilon^c(n)$ that described the parameter region around the bifurcation point when the Berry-Robnik formula did not work well. We checked numerically that the quantum mechanical data of the Berry-Robnik parameter in the region $\epsilon \gg \epsilon^c(n)$ accurately reproduced the classical volume ratio where the effective Planck constant was sufficiently smaller than the volume ratio of the island region. Therefore, we analytically and numerically evaluated the origin of the disagreement between the Berry-Robnik parameter and its counterpart the classical volume function in terms of the limit of resolution for the island tori by the quantum eigenstate.

Finally, we showed numerically that the Berry-Robnik parameter in the high energy region accurately approximated the classical volume ratio, and that it reproduced the cusp and the linear dependence more precisely in the high energy range than in the low energy range.

In this paper, we used as the classical Berry-Robnik parameter the relative measure $\rho_2(\mathrm{SOS})$ of the phase space components on the Poincaré surface of section (SOS). But it is the Liouville measure $\rho_2(\Gamma)$ on the energy surface $[\Gamma : H(\mathbf{q},\mathbf{p}) = E = \mathrm{const}]$ that must be used. According to the

Berry-Robnik theory [10], the Liouville measure should be equal to the quantum Berry-Robnik parameter in the strict semiclassical limit, so that we should discuss, for a given invariant component $\omega\,(=2)$, the relationship between $\rho_2(\Gamma)$ and ρ_2 (SOS), and their equivalence in our model. This relationship was derived by Meyer as follows [25,8,11,26],

$$\rho_\omega(\Gamma)=\frac{\int_\Gamma d\mathbf{q}d\mathbf{p}\,\delta(E-H(\mathbf{q},\mathbf{p}))\chi_\omega(\mathbf{q},\mathbf{p})}{\int_\Gamma d\mathbf{q}d\mathbf{p}\,\delta(E-H(\mathbf{q},\mathbf{p}))}$$

$$=\frac{\int_{\mathrm{SOS}} dX\,\tau(X)\chi_\omega(X)}{\int_{\mathrm{SOS}} dX\,\tau(X)}=\frac{\tau_\omega\int_{\mathrm{SOS}} dX\chi_\omega(X)}{\int_{\mathrm{SOS}} dX\,\tau(X)}$$

$$=C_\omega\rho_\omega(\mathrm{SOS}), \tag{8.1}$$

where $\chi_\omega(X)$ is the characteristic function of the invariant component defined as

$$\chi_\omega(X)=\begin{cases}1 & \text{if } X\in\omega\\ 0 & \text{if } X\in\overline{\omega}\end{cases}$$

and

$$C_\omega=\frac{\tau_\omega\int_{\mathrm{SOS}} dX}{\int_{\mathrm{SOS}}\tau(X)dX}=\frac{\tau_\omega}{\tau_{\mathrm{SOS}}} \tag{8.2}$$

$$=\frac{\int_{X\in\omega} dX+\int_{X\in\overline{\omega}} dX}{\int_{X\in\omega} dX+(1/\tau_\omega)\int_{X\in\overline{\omega}}\tau(X)dX}. \tag{8.3}$$

τ is the average time of recurrence of a trajectory to the SOS, which is constant for a given trajectory and thus also inside a given invariant component, e.g., $\tau_\omega=\tau(X\in\omega)=\mathrm{const}$, but changes from one component to another. One can see from Eq. (8.1) that $\rho_\omega(\Gamma)$ and ρ_ω (SOS) are not the same. However, in the neighborhood of the bifurcation point at δ_c, $C_\omega\simeq 1$ since each term in Eq. (8.3) satisfies the relation

$$\int_{X\in\omega} dX\gg\int_{X\in\overline{\omega}} dX,\quad \int_{X\in\omega} dX\gg\frac{1}{\tau_\omega}\int_{X\in\overline{\omega}}\tau(X)dX, \tag{8.4}$$

so that ρ_2 (SOS) approximates $\rho_2(\Gamma)$ very well in the neighborhood of the bifurcation point. This means that the characteristic structure of ρ_2 (SOS) at $\delta=\delta_c$, i.e., the cusp singularity and the linearity, is reproduced by the Liouville measure $\rho_2(\Gamma)$ on the energy surface as well.

The assumptions used in the derivation of the Berry-Robnik formula have not yet been validated from the theoretical viewpoint, although there is a lot of numerical evidence to verify the validity of the Berry-Robnik formula; Prosen and Robnik found that this formula approximates the numerical data in the far semiclassical regime better than the Brody distribution does [14,16,12]. Li and Robnik [18], Jacquod and Amiet [26], Prosen [15], and Makino, Harayama, and Aizawa [17] separated the energy levels into regular and irregular subclasses, and analyzed substatistics for each class in order to check the Berry-Robnik conjecture [10]. In this paper, by using the lemon billiard system, we showed that the Berry-Robnik parameter at the bifurcation point could not agree exactly with the classical volume ratio while in the finite energy range. However, in the high energy region, it reproduced well the characteristic structure of the classical volume ratio due to the bifurcation.

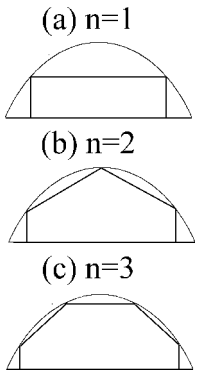

FIG. 13. A family of glancing periodic orbits that are subscripted by *n*.

APPENDIX A: BIFURCATION POINTS OF GLANCING PERIODIC ORBITS

Glancing periodic orbits with a period of $2(n+1), n=1,2,3,\ldots$, which are shown in Fig. 13, can exist in the parameter region

$$\delta_n\leqslant\delta\leqslant 1, \tag{A1}$$

where

$$\delta_n=d(n)-\sqrt{d(n)^2-1}, \tag{A2}$$

$$d(n)=1+1/\tan^2\left(\frac{\pi}{2}\frac{n}{n+1}\right),\quad n=1,2,3,\ldots. \tag{A3}$$

The critical values $\delta=\delta_n$ are special parameter points where the glancing periodic orbits, subscripted by *n*, appear suddenly from the singular regions on the boundary wall, $\phi=0$ and 0.5. In the parameter region Eq. (A1), the corresponding periodic points on the Poincaré surface of section are $(\phi(n),\sin\alpha(n))$,

$$\phi(n)=\frac{1}{4}\left[1-\frac{\alpha(n)}{\arctan[\sqrt{2\delta}/(1-\delta)]}\right], \tag{A4}$$

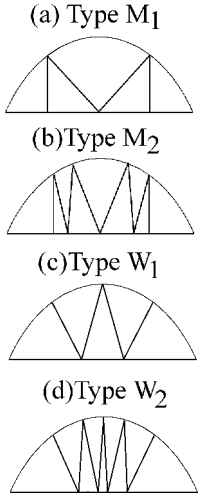

FIG. 14. Bouncing periodic orbits that are classified into two types of series, type M_n and type W_n $(n=1,2)$.

$$\alpha(n)=\frac{\pi}{2}\frac{n}{n+1}. \tag{A5}$$

APPENDIX B: BIFURCATION POINTS OF BOUNCING PERIODIC ORBITS

Tne bouncing periodic orbit with a period of $4n, n=1,2,3,\ldots$, can be classified into two series of typical types, i.e., type M_n and type W_n as shown in Figs. 14(a)–14(b) and Figs. 14(c)–14(d), respectively. Although we have not succeeded in deriving the bifurcation parameters of these periodic orbits in a systematic formulation of the subscripts n, some parameter values are shown below where the periodic orbits, classified by the subscript M_n or W_n, appear suddenly from the singular regions on the boundary wall, $\phi=0$ and 0.5. These periodic orbits can exist in the parameter region beyond δ_{M_n} or δ_{W_n}.

$$\delta_{M1}=2-\sqrt{3}=0.267\,949\,192\,4\ldots, \tag{B1}$$

$$\delta_{M2}=x\left(1-x=\frac{2x-(1-x)(1-x-\sqrt{1+x^2})}{\sqrt{2x+(1-x-\sqrt{1+x^2})}}\right)$$
$$=x(\text{a solution of the equation}\ \ 5x^4-40x^3+74x^2$$
$$-40x+5=0)$$
$$=0.178\,233\,390\,1\ldots$$
$$\vdots, \tag{B2}$$

$$\delta_{W1}=\frac{4-\sqrt{7}}{3}=0.451\,416\,229\ldots, \tag{B3}$$

$$\delta_{W2}=4-\sqrt{15}=0.127\,016\,653\,8\ldots, \tag{B4}$$

$$\delta_{W3}=x\left(\frac{x^2-4x+1}{\sqrt{1+x^2}}=\frac{-x^2+4x-1+(1-x)\sqrt{1+x^2}}{\sqrt{2x+(\sqrt{1+x^2}-(1-x))^2}}\right)$$
$$=x(\text{a solution of the equation}7x^6-112x^5+469x^4$$
$$-736x^3+469x^2-112x+7),$$
$$=0.094\,976\,632\,82\ldots$$
$$\vdots. \tag{B5}$$

APPENDIX C: EFFECTIVE PLANCK CONSTANT

Quantum mechanics with f degrees of freedom can resolve fine structures whose volume in the $2f$-dimensional phase space is larger than h^f or $(2\pi\hbar)^f$. h^f is called the Planck volume. The number of eigenenergy levels counted from the ground state, N, is obtained by applying the Thomas-Fermi approximation that each quantum state is associated with a phase-space volume h^f. One has therefore

$$N\simeq\frac{V}{h^f}, \tag{C1}$$

where V is the phase volume of the classical dynamical system. Equation (C1) is the Weyl term. The Planck volume normalized by the volume of the whole phase space, V, is expressed as

$$h_{\text{eff}}^f\equiv\frac{h^f}{V}\simeq\frac{1}{N}. \tag{C2}$$

For plane billiard systems with $f=2$ in particular, Eq. (C2) is rewritten as $h_{\text{eff}}^2\simeq 1/N$ so that the corresponding area in the tangential space (or in the Poincaré surface of section) is described by taking the square root of Eq. (C2) with $f=2$ as follows:

$$h_{\text{eff}}=\frac{h}{\sqrt{V}}\simeq\frac{1}{\sqrt{4n}}, \tag{C3}$$

where $N=4n$. $h_{\text{eff}}(n)$ is called the effective Planck constant. It gives the minimum area in the Poincaré surface of section whose structure can be resolved by the quantum eigenstate.

[1] M. V. Berry and M. Tabor, Proc. R. Soc. London, Ser. A **356**, 375 (1977).
[2] G. Casati, B. V. Chirikov, and I. Guarneri, Phys. Rev. Lett. **54**, 1350 (1985).
[3] O. Bohigas, M. J. Giannoni, and C. Schmit, Phys. Rev. Lett. **52**, 1 (1984).
[4] F. Borgonovi, G. Casati, and B. Li, Phys. Rev. Lett. **77**, 4744 (1996).
[5] M. Robnik, J. Phys. A **17**, 1049 (1984).
[6] T. H. Seligman, J. J. M. Verbaarschot, and M. R. Zirnbauer,

Phys. Rev. Lett. **53**, 215 (1984).
[7] T. Terasaka and T. Matsushita, Phys. Rev. A **32**, 538 (1985).
[8] H. D. Meyer, E. Haller, H. Köppel, and L. S. Cederbaum, J. Phys. A **17**, L831 (1984).
[9] V. Lopac, I. Mrkonjić, and D. Radić, Phys. Rev. E **59**, 303 (1999).
[10] M. V. Berry and M. Robnik, J. Phys. A **17**, 2413 (1984).
[11] M. Robnik, Nonlin. Phenom. Complex Syst. **1**, 1 (1998).
[12] M. Robnik and T. Prosen, J. Phys. A **30**, 8787 (1997).
[13] T. Prosen and M. Robnik, J. Phys. A **26**, 2371 (1993).
[14] T. Prosen and M. Robnik, J. Phys. A **27**, 8059 (1994).
[15] T. Prosen, Physica D **91**, 244 (1996).
[16] T. Prosen, J. Phys. A **31**, 7023 (1998).
[17] H. Makino, T. Harayama, and Y. Aizawa, Prog. Theor. Phys. Suppl. **139**, 477 (2000).
[18] B. Li and M. Robnik, J. Phys. A **28**, 4843 (1995).
[19] H. Makino, T. Harayama, and Y. Aizawa, Phys. Rev. E **59**, 4026 (1999).
[20] E. J. Heller and S. Tomsovic, Phys. Today **46(7)**, 38 (1993).
[21] S. Ree and L. E. Reichl, Phys. Rev. E **60**, 1607 (1999).
[22] G. D. Birkhoff, *Dynamical Systems* (American Mathematical Society, Providence, RI, 1927; reprinted 1996).
[23] T. Harayama, A. Shudo, and T. Tasaki, Nonlinearity **12**, 1113 (1999).
[24] R. S. MacKay and J. D. Meiss, Phys. Lett. **92A**, 98 (1983).
[25] H. D. Meyer, J. Chem. Phys. **84**, 3147 (1985).
[26] P. Jacquod and J. P. Amiet, J. Chem. Phys. **28**, 4799 (1995).